

# Spectroscopic Diagnosis of Excited-State Aromaticity: Capturing Electronic Structures and Conformations upon Aromaticity Reversal

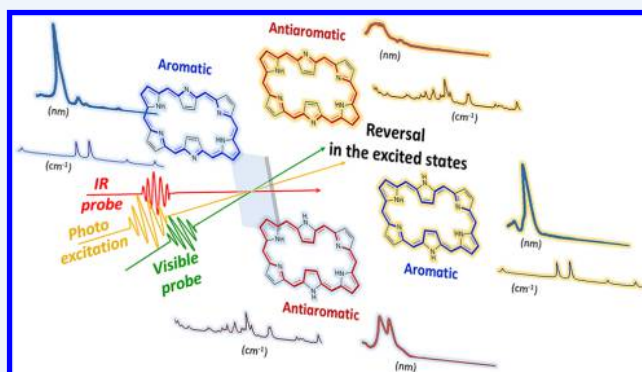
Juwon Oh, Young Mo Sung,<sup>†</sup> Yongseok Hong, and Dongho Kim\*<sup>✉</sup>

Spectroscopy Laboratory for Functional  $\pi$ -Electronic Systems and Department of Chemistry, Yonsei University, Seoul 120-749, Korea

**CONSPECTUS:** Aromaticity, the special energetic stability derived from cyclic  $[4n + 2]\pi$ -conjugated electronic structures, has been the topic of intense interest in chemistry because it plays a critical role in rationalizing molecular stability, reactivity, and physical/chemical properties. Recently, the pioneering work by Colin Baird on aromaticity reversal, postulating that aromatic (antiaromatic) character in the ground state reverses to antiaromatic (aromatic) character in the lowest excited triplet state, has attracted much scientific attention. The completely reversed aromaticity in the excited state provides direct insight into understanding the photophysical/chemical properties of photoactive materials. In turn, the application of aromatic molecules to photoactive materials has led to numerous studies revealing this aromaticity reversal. However, most studies of excited-state aromaticity have been based on the theoretical point of view. The experimental evaluation of aromaticity in the excited state is still challenging and strenuous because the assessment of (anti)aromaticity with conventional magnetic, energetic, and geometric indices is difficult in the excited state, which practically restricts the extension and application of the concept of excited-state aromaticity.

Time-resolved optical spectroscopies can provide a new and alternative avenue to evaluate excited-state aromaticity experimentally while observing changes in the molecular features in the excited states. Time-resolved optical spectroscopies take advantage of ultrafast laser pulses to achieve high time resolution, making them suitable for monitoring ultrafast changes in the excited states of molecular systems. This can provide valuable information for understanding the aromaticity reversal.

This Account presents recent breakthroughs in the experimental assessment of excited-state aromaticity and the verification of aromaticity reversal with time-resolved optical spectroscopic measurements. To scrutinize this intriguing and challenging scientific issue, expanded porphyrins have been utilized as the ideal testing platform for investigating aromaticity because they show distinct aromatic and antiaromatic characters with aromaticity-specific spectroscopic features. Expanded porphyrins exhibit perfect aromatic and antiaromatic congener pairs having the same molecular framework but different numbers of  $\pi$  electrons, which facilitates the study of the pure effect of aromaticity by comparative analyses. On the basis of the characteristics of expanded porphyrins, time-resolved electronic and vibrational spectroscopies capture the changes in electronic structure and molecular conformations driven by the change in aromaticity and provide clear evidence for aromaticity reversal in the excited states. The approaches described in this Account pave the way for the development of new and alternative experimental indices for the evaluation of excited-state aromaticity, which will enable overarching and fundamental comprehension of the role of (anti)aromaticity in the stability, dynamics, and reactivity in the excited states with possible implications for practical applications.



Time-resolved optical spectroscopies can provide a new and alternative avenue to evaluate excited-state aromaticity experimentally while observing changes in the molecular features in the excited states. Time-resolved optical spectroscopies take advantage of ultrafast laser pulses to achieve high time resolution, making them suitable for monitoring ultrafast changes in the excited states of molecular systems. This can provide valuable information for understanding the aromaticity reversal.

This Account presents recent breakthroughs in the experimental assessment of excited-state aromaticity and the verification of aromaticity reversal with time-resolved optical spectroscopic measurements. To scrutinize this intriguing and challenging scientific issue, expanded porphyrins have been utilized as the ideal testing platform for investigating aromaticity because they show distinct aromatic and antiaromatic characters with aromaticity-specific spectroscopic features. Expanded porphyrins exhibit perfect aromatic and antiaromatic congener pairs having the same molecular framework but different numbers of  $\pi$  electrons, which facilitates the study of the pure effect of aromaticity by comparative analyses. On the basis of the characteristics of expanded porphyrins, time-resolved electronic and vibrational spectroscopies capture the changes in electronic structure and molecular conformations driven by the change in aromaticity and provide clear evidence for aromaticity reversal in the excited states. The approaches described in this Account pave the way for the development of new and alternative experimental indices for the evaluation of excited-state aromaticity, which will enable overarching and fundamental comprehension of the role of (anti)aromaticity in the stability, dynamics, and reactivity in the excited states with possible implications for practical applications.

## INTRODUCTION

Aromaticity is one of the most fundamental concepts in chemistry. In 1931, Hückel proposed the pivotal model of aromaticity: planar cyclic  $\pi$ -conjugated molecules with  $4n + 2$   $\pi$  electrons are energetically stable and aromatic, whereas molecules with  $4n$   $\pi$  electrons are energetically unstable and antiaromatic.<sup>1</sup> Since (anti)aromaticity is associated with the reactivity and physical/chemical responses of molecules, the fundamental relationship between aromaticity and the properties of systems, as well as the possibility for applications, has long been studied.

Recently, the pioneering prediction of excited-state aromaticity reversal by Colin Baird has drawn much attention. On the basis of perturbation molecular orbital theory, he postulated

that the Hückel aromatic or antiaromatic character in the ground state becomes reversed in the lowest  $\pi, \pi^*$  triplet state (Figure 1a).<sup>2,3</sup> Considering annulenes in the lowest triplet state in a molecular interaction with two carbonyl radicals with odd numbers of  $\pi$  electrons, a  $[4n]\pi$ -electronic system, such as cyclooctatetraene, becomes energetically stable. In the same way,  $[4n + 2]\pi$ -electron conjugated rings such as benzene become unstable. This concept of excited-state aromaticity reversal is highly significant because completely reversed aromaticity in the excited state provides crucial insight into photostability, photoreactivity, and its application to photo-

Received: December 20, 2017

Published: March 6, 2018

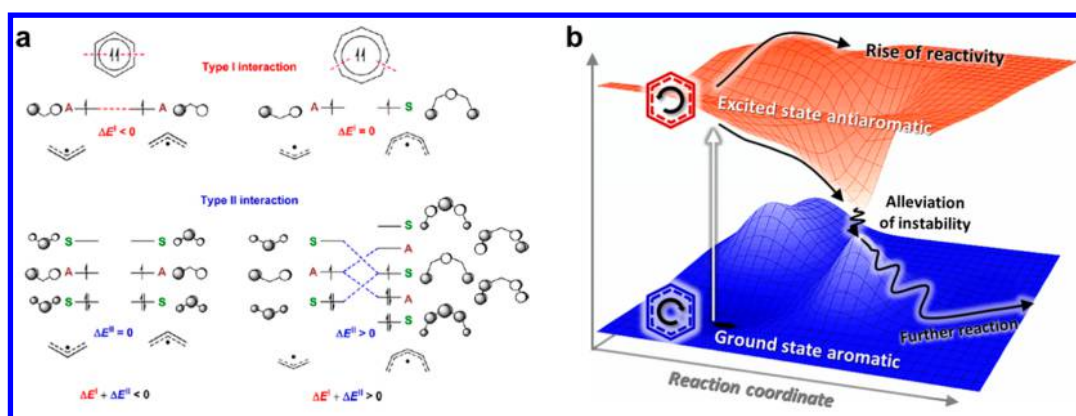


**Figure 1.** (a) Scheme displaying type I ( $\Delta E^I$ ) and type II ( $\Delta E^{II}$ ) interactions between the  $\pi$  orbitals of radical fragments that when combined yield triplet biradical benzene and cyclooctatetraene. The nonzero type I and II interactions are marked with dashed lines in red and blue, respectively. The symmetry or antisymmetry of a  $\pi$  MO with respect to a bisecting mirror plane is labeled with an S or A, respectively. A positive total interaction corresponds to a stabilization upon cyclization and a triplet-state aromatic ring, whereas a negative total interaction corresponds to a destabilization upon cyclization and a triplet-state antiaromatic ring. Reprinted from ref 3. Copyright 2014 American Chemical Society. (b) Schematic diagram of photoinduced properties and potential energy induced by aromaticity reversal.<sup>9,10</sup>

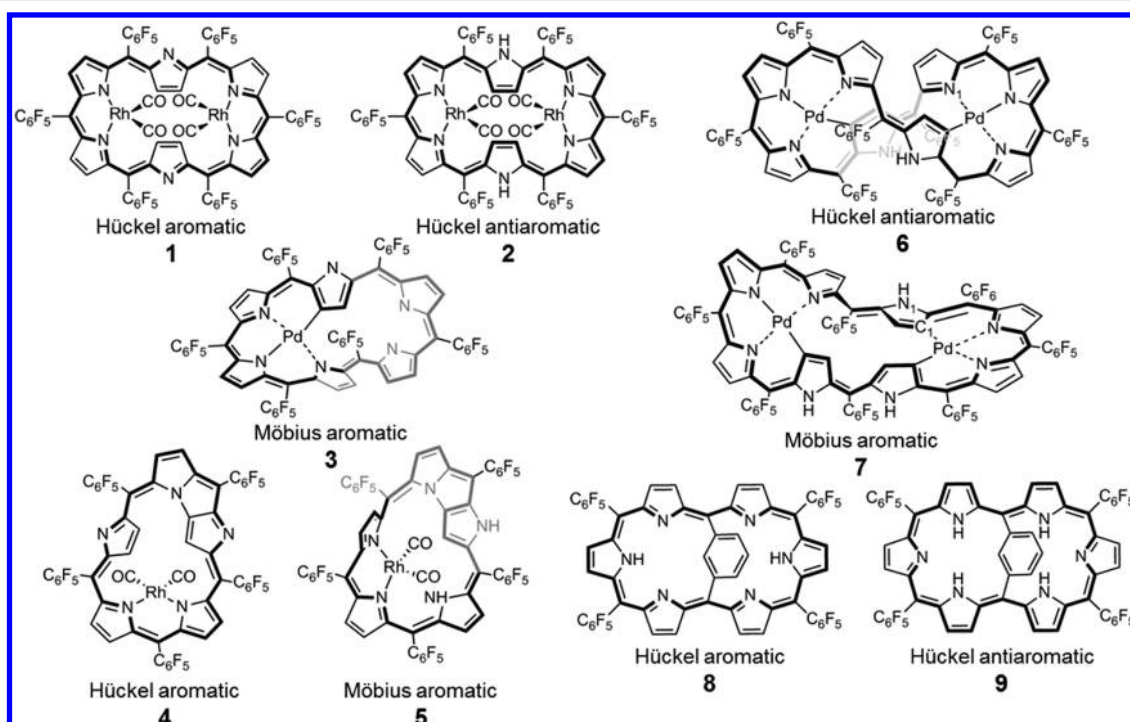


**Figure 2.** Structures of expanded porphyrins.

synthetic mechanisms and photoactive materials (Figure 1b).<sup>3–10</sup> In this regard, enormous theoretical effort has been devoted to the verification of aromaticity reversal in the excited state using various computational analyses.<sup>3</sup>

However, despite extensive theoretical studies, experimental substantiation of aromaticity reversal is still on the infantile level. The majority of experimental studies have investigated only intermediates, chemical reactivity, and isomerization.<sup>3</sup> The practical inaccessibility in measuring the conventional geometric, magnetic, and energetic indices of aromaticity in the excited state using techniques such as NMR spectroscopy and X-ray crystallography has heavily restricted the empirical investigation of excited-state aromaticity. Thus, the need for effective experimental approaches to evaluate excited-state aromaticity should be addressed.

Recently, as a new and unconventional method, time-resolved spectroscopic measurements have shed light on excited-state aromaticity.<sup>5,11–16</sup> Optical spectroscopies in the visible and near-IR (NIR) region are some of the most effective methods for characterizing the electronic and vibrational features of molecules in the ground state, and the combination with ultrafast laser pulses allows for the characterization of molecular features in the excited states.<sup>17,18</sup> Thus, these time-resolved optical spectroscopic measurements can monitor ultrafast changes in the transient excited states, enabling investigation of significant clues about excited-state aromaticity. Kim, Osuka, and co-workers have devoted continuous effort to developing new experimental indices to estimate (anti)-aromaticity on the basis of spectroscopic features.<sup>19–21</sup> They have focused on expanded porphyrins, i.e., macrocycles

containing more than four pyrrole-related rings (Figure 2). The expanded porphyrins show distinct aromaticity-dependent physical and chemical properties and serve as comparable sets of aromatic and antiaromatic species; thus, these compounds facilitate revealing clear correlations between spectroscopic features and (anti)aromaticity.<sup>20,21</sup> The trailblazing works by Kim, Osuka, and co-workers were extended to aromaticity in the excited state and opened new possibilities for studies of excited-state aromaticity using time-resolved spectroscopy. Time-resolved electronic and vibrational absorption spectroscopies capture the transient changes of electronic structures and molecular conformations in the excited states derived from changes in aromaticity, which provide clear evidence for aromaticity reversal. In this regard, Hada et al.<sup>22</sup> also captured periodic structural dynamics induced by excited-state aromaticity with time-resolved electron diffraction measurements and optical spectroscopy.

This Account will summarize recent breakthroughs in unraveling excited-state aromaticity by focusing on the time-resolved optical spectroscopies as effective approaches to verify the concept of aromaticity reversal. First, aromaticity reversal in expanded porphyrins having planar, Möbius, and figure-of-eight geometries is addressed by capturing their altered  $\pi$ -electronic structures in the lowest triplet state.<sup>11–13</sup> The next section discusses aromaticity reversal in the excited singlet states.<sup>14</sup> Lastly, time-resolved vibrational (IR) spectroscopy is introduced as an approach to monitor aromaticity-driven geometrical changes triggered by aromaticity reversal.<sup>5,15</sup> Thus, the time-resolved spectroscopic measurements are unconventional but effective approaches to investigate excited-state aromaticity.

### EVALUATION OF AROMATICITY BASED ON THE OPTICAL SPECTROSCOPIC FEATURES OF EXPANDED PORPHYRINS

Expanded porphyrins have attracted intense attention over the past few decades. Various sizes and types of expanded porphyrins have been synthesized, and their potential applications have been demonstrated, such as their utilization in photodynamic therapy and anion recognition as well as their use as functional NIR dyes for nonlinear optics.<sup>23–26</sup>

Among various scientific subjects on expanded porphyrins, aromaticity is one of the major issues because they display stable and distinct aromatic and antiaromatic characteristics. Moreover, expanded porphyrins exhibit aromatic  $[4n + 2]$ - and antiaromatic  $[4n]\pi$ -conjugated congener pairs that have the same molecular framework but differ in the number of  $\pi$  electrons, making them ideally suited for studying the pure effect of aromaticity.<sup>11–14</sup> In this regard, Kim, Osuka, and co-workers have made extensive efforts to study the aromaticity of expanded porphyrins in order to develop experimental aromaticity indices.<sup>4,19–21</sup> They have focused on distinct aromaticity-dependent optical spectroscopic features of expanded porphyrins.<sup>20</sup> Aromatic expanded porphyrins show intense and distinct B- and Q-like bands in the absorption spectra, fluorescence behaviors with relatively long excited-state lifetimes, and large two-photon absorption values. On the other hand, antiaromatic expanded porphyrins display broad and weak bands with absorption tailing in the NIR region in their absorption spectra, no fluorescence behavior with relatively short excited-state lifetimes, and small two-photon absorption values. These aromaticity-dependent features arise from the characteristic  $\pi$ -electronic structures of aromatic and antiaromatic expanded porphyrins, which are directly reflected in

their absorption spectra (Figure 3);<sup>21,27–29</sup> aromatic expanded porphyrins possess four degenerate frontier molecular orbitals

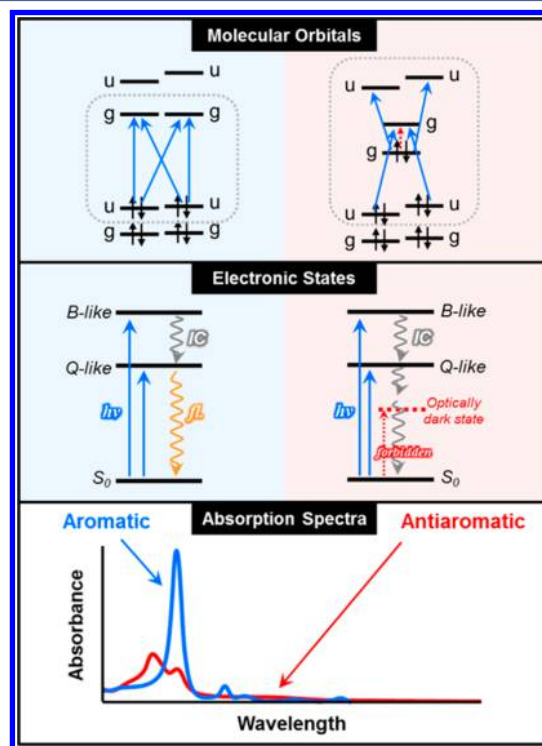


**Figure 3.** Aromaticity-dependent optical spectroscopic properties and  $\pi$ -electronic structures of expanded porphyrins.

(FMOs), namely, HOMO–1 to LUMO+1, and configuration interaction between the four FMOs results in the intense B-like and weak Q-like absorption bands.<sup>27</sup> On the other hand, the distorted structure of antiaromatic expanded porphyrins breaks the degeneracy of the frontier levels, leading to a one-photon-forbidden gerade HOMO to gerade LUMO transition, and the configuration interaction between six FMOs (HOMO–2 to LUMO+2) engenders broad, weak, and ill-defined absorption bands with characteristic tailing in the NIR region.<sup>21,28,29</sup> These spectroscopic features serve as indices for the evaluation of aromaticity and can be extended as the key foundation for time-resolved spectroscopic measurements to scrutinize excited-state aromaticity.

### MONITORING CHANGES IN ELECTRONIC STRUCTURE IN THE LOWEST TRIPLET STATE AND AROMATICITY REVERSAL

As described above, the absorption spectral features, such as band shapes with or without the dark state in the NIR region, are a direct consequence of their aromaticity-dependent  $\pi$ -electronic structures.<sup>4,21,28,29</sup> These distinct features of expanded porphyrins directly support the experimental evaluation of excited-state aromaticity.

For an experimental demonstration of aromaticity reversal in the lowest triplet state by the spectroscopic features, metalated expanded porphyrins, which efficiently populate the triplet state by the heavy-metal effect, were studied.<sup>11–13</sup> First, bis-(rhodium) [26]hexaphyrin **1** (aromatic) and [28]hexaphyrin **2** (antiaromatic) were spotlighted to unveil aromaticity reversal in the lowest triplet state (Figure 4).<sup>11</sup> Their absorption spectra exhibit the characteristic features of typical aromatic and

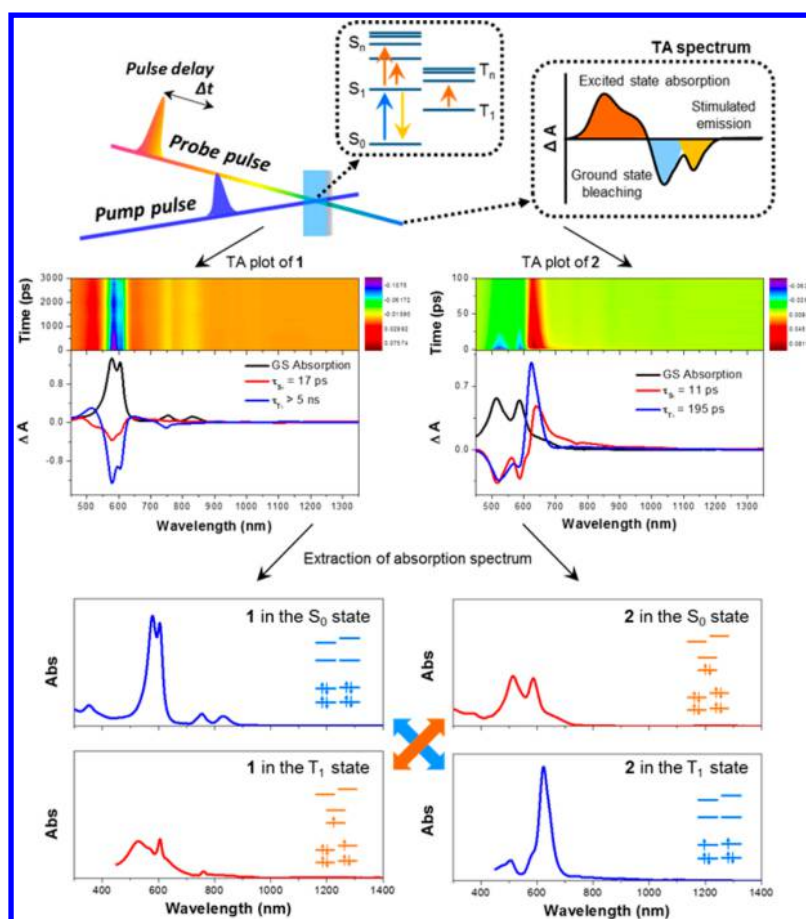


**Figure 4.** (top) Scheme for TA spectroscopy. (middle) TA contour maps and ground-state absorption and decay-associated spectra of 1 and 2. (bottom) Ground- and lowest-triplet-state absorption spectra of 1 and 2.

antiaromatic expanded porphyrins. **1** shows intense B-like bands with distinct Q-like bands, whereas **2** displays broad and weak absorption spectra with a smeared tail in the NIR region, indicating the presence of the dark state. These absorption spectral features are in line with the aromatic and antiaromatic natures of **1** and **2**, respectively. Here, the time-resolved electronic absorption measurement by femtosecond transient absorption (fs-TA) spectroscopy observed the absorption spectral changes in the lowest triplet state of these hexaphyrins. TA spectroscopy measures an absorbance difference ( $\Delta A$ ) that is composed of positive excited-state absorption and stimulated emission signals from the excited-state species with a negative ground-state bleaching signal from the reduced ground-state species.<sup>4</sup> This indicates that the subtraction of the ground-state absorption spectrum from the transient absorption spectrum allows the extraction of the excited-triplet-state absorption spectrum.<sup>11</sup> The estimated absorption spectra of **1** and **2** in the lowest triplet state are interconvertible to those for the ground state. The estimated triplet-state absorption spectrum of **1** exhibits broader and weaker absorption peaks compared with the ground-state absorption spectrum, while **2** presents a sharper and intensified excited-state absorption spectrum. Considering the aromaticity-dependent spectral features, these interconvertible absorption spectra between **1** and **2** indicate switching of the  $\pi$ -electronic structures and reversed aromaticity in the lowest triplet state.

Quantum calculation analyses provide in-depth comprehension of this correlation of the reversal of aromaticity with the

change in the absorption spectral features of aromatic **1** and antiaromatic **2** between the ground and lowest triplet states.<sup>11</sup> The calculated vertical excitation energies of **1** in the ground state, which show a nice accordance with the ground-state absorption spectrum, arise from the configuration interaction between the four degenerate FMOs, the unique  $\pi$ -electronic structure of aromatic expanded porphyrins. On the other hand, the vertical excitation energy calculation results for **2** in the ground state result from the configuration interaction between the six FMOs, representing the  $\pi$ -electronic structure of antiaromatic expanded porphyrins. The vertical excitation energies calculated for **1** and **2** in the lowest triplet state display the fully contrasting results, where the lowest-triplet-state absorption spectra of **1** and **2** are evaluated with the configuration interaction of the six nondegenerate and four degenerate FMOs, respectively.

The combination of the interconvertible spectral features of aromatic **1** and antiaromatic **2** with theoretical indices to quantify aromatic and antiaromatic character, including the nucleus-independent chemical shift (NICS) and harmonic oscillator model of aromaticity (HOMA), constitutes convincing experimental evidence for aromaticity reversal.<sup>11</sup> The contrasting NICS and HOMA results for **1** and **2** for the lowest triplet state compared with those for the ground state describe well the aromaticity reversal in the lowest triplet state. Consequently, the interconvertible absorption spectral features of **1** and **2** in the ground and lowest triplet states provide

experimental testimony in favor of Baird's aromaticity prediction.

In conjunction with the aromaticity reversal in the lowest triplet state in planar topologies, this concept of excited-state aromaticity has been extended to molecules possessing complex topologies, such as Möbius and figure-of-eight structures. In this regard, the expanded porphyrins **3**, **4**, and **5** were in the limelight for aromaticity reversal in Möbius aromatic systems.<sup>12</sup> The X-ray crystallographic and <sup>1</sup>H NMR results clearly delineated the aromatic natures of **3** and **5** arising from the presence of 28 and 24  $\pi$  electrons, as shown by their Möbius geometries. The previous synthetic study revealed that the pentaphyrin **4**, showing a planar 22- $\pi$ -electron Hückel aromatic nature, is a congener of **5**. According to the distinct Hückel and Möbius aromatic natures of **3**, **4**, and **5**, they show the conspicuous absorption spectral features, including intense B-like and relatively small Q-like bands (Figure 5). These spectral

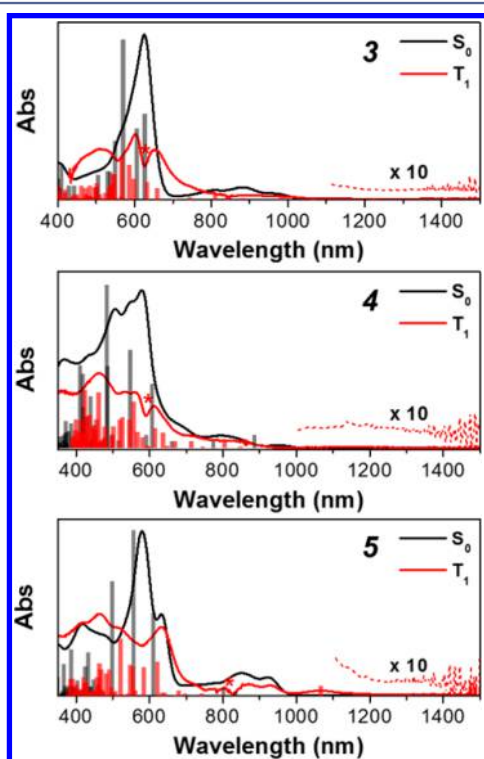


**Figure 5.** Ground-state (gray line) and lowest-triplet-state (red line) absorption spectra of (top) **3**, (middle) **4**, and (bottom) **5** with vertical energy transition plots for the ground states (gray columns) and triplet states (red columns).

features illustrate that the Hückel and Möbius aromatic expanded porphyrins have similar  $\pi$ -electronic structures even though there is a large geometrical difference. This is understandable considering that Möbius aromaticity is also postulated on the basis of Hückel molecular orbital theory,<sup>30</sup> which suggests that Möbius aromaticity should also be reversed in the lowest triplet state. In this regard, the fs-TA measurements captured the changes in the  $\pi$ -electronic structures of **3**, **4**, and **5** in the lowest triplet state. The extracted lowest-triplet-state absorption spectra of **3**, **4**, and **5** show relatively weak and broad absorption peaks with a long tail in the NIR region. These spectral features are analogous to those of antiaromatic **2**, which gives the direct insight that Möbius aromatic character in the ground state is reversed into

Möbius antiaromatic character in the lowest triplet state in the same manner as Hückel (anti)aromaticity.

The quantum calculation analyses give a detailed description of the changes in the absorption spectral features of **3**, **4**, and **5** between the ground and lowest triplet states in association with the excited-state aromaticity.<sup>12</sup> The vertical excitation energy calculation results for **3**, **4**, and **5** in the ground state represent well that their main electronic transitions arise from the configuration interaction between the four degenerate FMOs, the unique  $\pi$ -electronic structure of aromatic expanded porphyrins. On the other hand, for **3**, **4**, and **5** in the lowest triplet state, the configuration interaction between the six FMOs delineates the broad, weak, and tailing features in their lowest-triplet-state absorption spectra. These in-depth spectral analyses correspond with other calculated aromaticity indices, such as mean-plane deviation, HOMA, and NICS results,<sup>12</sup> affording convincing evidence for the reversal of Möbius aromaticity in the ground state into Möbius antiaromaticity in the lowest triplet state.

In sequence, the excited-state aromaticity in a more complicated topology, the figure-of-eight topology, was unraveled by fs-TA measurements focused on a pair of bis(palladium) octaphyrins (**6** and **7**).<sup>13</sup> Interestingly, although they have the same number of  $\pi$  electrons, their different structures cause **6** and **7** to exhibit double-sided Hückel antiaromatic and single-sided Möbius aromatic characters, respectively. The aromaticity of **7** and antiaromaticity of **6** are reflected in their absorption spectra; aromatic **7** exhibits strong B-like and weak Q-like bands, while antiaromatic **6** displays weak, broad bands in the visible region with smeared NIR bands indicating the optically dark state. Compared with the ground-state absorption spectra, the lowest-triplet-state absorption spectra of **6** and **7** show the contrasting spectral features. The absorption bands of **7** in the lowest triplet state become reduced and broadened compared with those in the ground state. In the case of **6**, the maximum extinction coefficients are increased and the peaks become sharpened compared with the ground-state absorption spectrum. These spectral changes of **6** and **7** between the ground and lowest triplet states are in the same line as those of **1** and **2**, which indicates the reversed aromaticity in the lowest triplet state. Moreover, this suggests that regardless of the molecular topology, the aromatic and antiaromatic natures springing from cyclic  $\pi$  conjugation are reversed in the lowest triplet state.

These time-resolved electronic absorption spectroscopic results, the absorption spectral changes, and the theoretical analyses of  $\pi$ -electronic structures clearly demonstrate the aromaticity reversal of expanded porphyrins in the lowest triplet state. This suggests that the time-resolved absorption spectral analysis is an effective approach for investigation of excited-state aromaticity and will provide more fruitful information on aromaticity reversal and its role in the photophysical/chemical properties.

## ■ MONITORING CHANGES IN ELECTRONIC STRUCTURE IN THE EXCITED SINGLET STATES AND AROMATICITY REVERSAL

Aromaticity reversal in the excited singlet states, by extension of Baird's aromaticity prediction, has attracted much attention because the excited singlet states are inevitable intermediate states by molecular excitation. However, although the aromaticity reversal in the excited singlet states was postulated on the basis of the similarity of electronic features between the

excited singlet and triplet states,<sup>31</sup> its experimental and even theoretical substantiation is still limited to only scant examples that are not clearly identified to date.<sup>9,32–34</sup> The computational adversities as well as restrictions on quantitative experimental analyses for the excited singlet states have resulted in large difficulties and inaccuracies in the analysis of excited-singlet-state aromaticity. This highlights the need for discrete experimental verification of excited-singlet-state aromaticity.

The capture of absorption spectral changes by fs-TA measurements provided clues to overcome these difficulties in experimental and theoretical studies of excited-singlet-state aromaticity. Here, phenylene-bridged hexaphyrin congeners, aromatic **8** and antiaromatic **9**, were spotlighted, allowing measurement of the pure (anti)aromatic effect in the excited singlet states.<sup>14</sup> As typical aromatic and antiaromatic expanded porphyrins, **8** exhibits a ground-state absorption spectrum showing strong B-like bands with discrete Q-like bands while in **9** exhibits a spectrum with relatively broad and weak bands in the visible region and a featureless tail in the NIR region (Figure 6). These characteristic absorption spectral features of

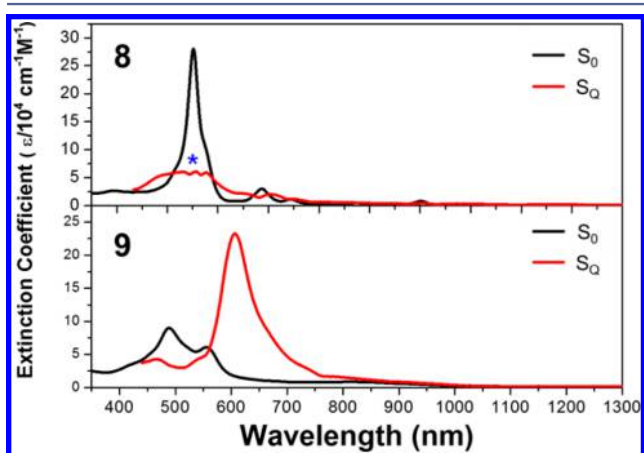


**Figure 6.** Ground- and excited-singlet-state absorption spectra of **8** and **9**. Reprinted from ref 14. Copyright 2015 American Chemical Society.

**8** and **9** explicitly delineate their aromaticity-dependent  $\pi$ -electronic structures. Similar to the triplet absorption extraction, the TA measurements for **8** and **9** allowed monitoring of the changes in the absorption spectral features reflecting  $\pi$ -electronic structures in the excited singlet state, which enabled their excited-singlet Q-like state ( $S_Q$ ) absorption spectra to be estimated.<sup>14</sup> Contrary to their ground-state absorption spectra, the absorption spectrum of **8** in the  $S_Q$  state displays broad B-like bands and a featureless tail with reduced extinction coefficients, while that of **9** exhibits intensified and sharpened B- and Q-like bands. Although these characteristics in the excited singlet state are not fully supported theoretically because of the computational challenges related to assessing the excited singlet state, particularly for macrocyclic systems,<sup>9</sup> the interconvertible spectral features of **8** and **9** between the ground and  $S_Q$  states directly represent the aromaticity-driven changes in the  $\pi$ -electronic structures in the expanded porphyrins. In other words, (anti)aromaticity is reversed not only in the lowest triplet state but in the excited singlet state. This evaluation of excited-singlet-state aromaticity suggests that to overcome the current difficulties in the study of excited-singlet-state aromaticity, measurement of the absorption

spectral changes by the TA spectroscopy is an effective method to afford reliable evidence for evaluating excited-singlet-state aromaticity.

### ■ VIBRATIONAL MODE ANALYSIS TO PROBE AROMATICITY-DRIVEN STRUCTURAL CHANGES IN THE EXCITED STATE

Among representative indices for evaluation of aromaticity, such as magnetism, energy, and electronic structure, molecular geometry is one of the fundamental properties to decide aromaticity and antiaromaticity. In various geometrical indices, molecular conformation is one of the most representative characteristics showing aromaticity dependence. Electronically unstable antiaromatic molecules tend to become stable via structural distortions, whereas aromatic molecules adopt planar and rigid geometries to achieve more effective  $\pi$  conjugation.<sup>5,35</sup> However, there is a practical difficulty in measuring the conventional geometric indices, such as NMR and X-ray crystal data, as well as magnetic and energetic ones in the excited state.

Alternatively, vibrational modes, which are closely associated with molecular structures as well as  $\pi$ -electron delocalization, can provide crucial information on aromaticity in the excited states as well as the ground state. Extensive efforts have been devoted to revealing the relationship between aromaticity and vibrational modes based on molecular geometries.<sup>31,36</sup> Judging from the aromaticity-dependent molecular conformation, the reversed aromaticity in the excited state triggers a conformational change, which is accompanied by modulation of the vibrational modes. Thus, monitoring of the vibrational changes facilitates an evaluation of excited-state aromaticity.

Recently, Kim and colleagues employed time-resolved IR (TRIR) spectroscopy to shed light on excited-state aromaticity from the geometrical point of view.<sup>5,15</sup> They focused on the C=C stretching vibrational modes of expanded porphyrins. Because of the vibrational selection rule for a change in dipole moment, the IR activity of C=C stretching vibration modes, which are the main constituents of cyclic  $\pi$  conjugation and usually appear at 1300–1700  $\text{cm}^{-1}$ , is sensitive to conformational distortions (Figure 7).<sup>5</sup> Here, aromatic molecules possess planar structures for more energetic stabilization via effective  $\pi$  conjugation. Along the planar structures, the C=C stretching modes vibrate symmetrically in the in-plane direction. Because these vibrational modes accompany a negligible change in the dipole moment, these vibrations are IR-forbidden, leading to simple and attenuated IR spectral features in the 1300–1700  $\text{cm}^{-1}$  region. On the other hand, antiaromatic systems show distorted structures due to their energetic instability. Along the distorted structures, the C=C stretching modes occur asymmetrically in the out-of-plane direction. These vibrational motions provoke a change in the dipole moment and become IR-active, resulting in large IR intensities. This indicates that the IR spectral features in the 1300–1700  $\text{cm}^{-1}$  region provide geometrical information associated with aromaticity, and TRIR measurements can monitor changes in the vibrational modes and conformational distortions in the excited states driven by the reversal of aromaticity.

From this perspective, the C=C stretching vibration modes of aromatic **1** and antiaromatic **2** were spotlighted. The Fourier transform IR (FTIR) spectra of **1** and **2** show two intense bands in the 1400–1550  $\text{cm}^{-1}$  region with a small peak at 1650  $\text{cm}^{-1}$  arising from local C=C stretching modes of the asymmetric *meso*-pentafluorophenyl ( $\text{C}_6\text{F}_5$ ) substituents (Figure 8a,b).<sup>15</sup> Aside from these common IR bands, **1** and **2**

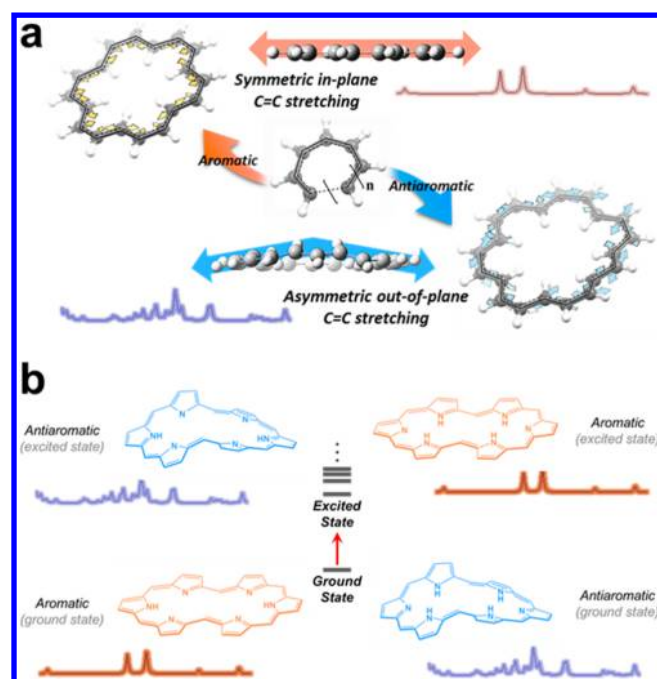


**Figure 7.** Schemes for (a) aromaticity-dependent IR activity in aromatic/antiaromatic molecular systems and (b) the reversal of aromaticity and accompanying structural and IR spectral changes.

exhibit contrasting spectral features in the 1300–1700  $\text{cm}^{-1}$  region: the FTIR spectrum of **1** displays negligible IR bands, while that of **2** shows additional distinct bands at 1350, 1570, and 1610  $\text{cm}^{-1}$ . On the basis of the correlation between the aromaticity and the C=C stretching vibrational modes, the contrasting IR spectral features illustrate that the ground-state structure of **1** is symmetric and planar and that of **2** is rather distorted. The TRIR spectra of **1** and **2** reflect their IR spectral

changes in the lowest triplet state. Except for the IR bands from the  $\text{C}_6\text{F}_5$  substituents, the TRIR spectra of **1** show weak ground-state IR bleaching bands with distinct excited-state IR absorption bands. In the case of **2**, the ground-state IR bleaching bands are strong while the excited-state IR absorption bands are weak and featureless. Since the ground-state IR bleaching bands are well matched with the FTIR spectra, the lowest-triplet-state IR spectra of **1** and **2** are directly estimated on the basis of the excited-state IR absorption bands and show interconvertible spectral features with their IR spectra for the ground state. These reversed IR spectral features in the lowest triplet state are interpreted on the basis of the IR activity of C=C stretching modes that the structures of **1** and **2** become distorted and planar, respectively, in the lowest triplet state. These changes in IR spectral features and molecular conformations are in accordance with the aromaticity reversal of **1** and **2** in the lowest triplet state and demonstrate the aromaticity-driven structural changes in the lowest triplet state.<sup>11</sup>

In addition to the lowest-triplet-state aromaticity, TRIR measurements on aromatic **8** and antiaromatic **9** provide clear evidence revealing the aromaticity reversal in the excited singlet states (Figure 8c,d).<sup>5</sup> The FTIR spectra of **8** and **9** show spectral features similar to those of aromatic **1** and antiaromatic **2**, including the common IR bands from the asymmetric *meso*- $\text{C}_6\text{F}_5$  substituents, strong bands at 1485 and 1520  $\text{cm}^{-1}$ , and weak bands at 1430 and 1650  $\text{cm}^{-1}$ . Although the excited-state lifetimes of **8** and **9** are different from those of **1** and **2** because of efficient intersystem crossing by the rhodium atoms in the latter, the TRIR spectra of **8** and **9** are also analogous with those of **1** and **2**. Since **1**, **2**, **8**, and **9** possess the same *meso*-hexakis(pentafluorophenyl)hexaphyrin molecular framework, differing only in the central rhodium atoms and phenylene bridge, this spectral similarity indicates that most of the C=C stretching vibrational modes in 1300–1700  $\text{cm}^{-1}$  region originate from the main  $\pi$ -conjugation pathway of the

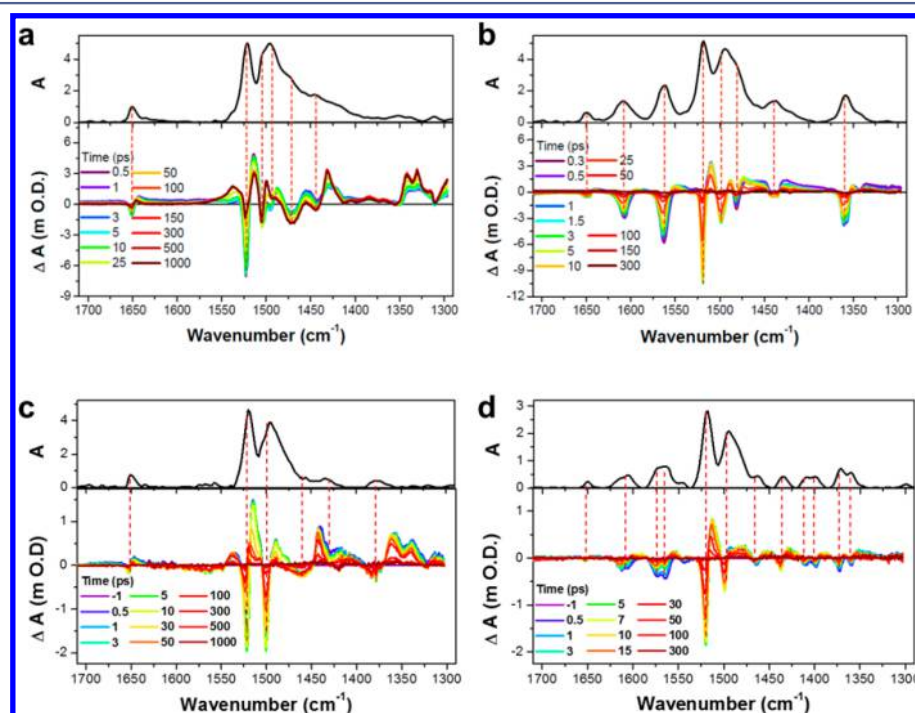


**Figure 8.** (top) FTIR and (bottom) TRIR spectra of (a) **1**, (b) **2**, (c) **8**, and (d) **9**.

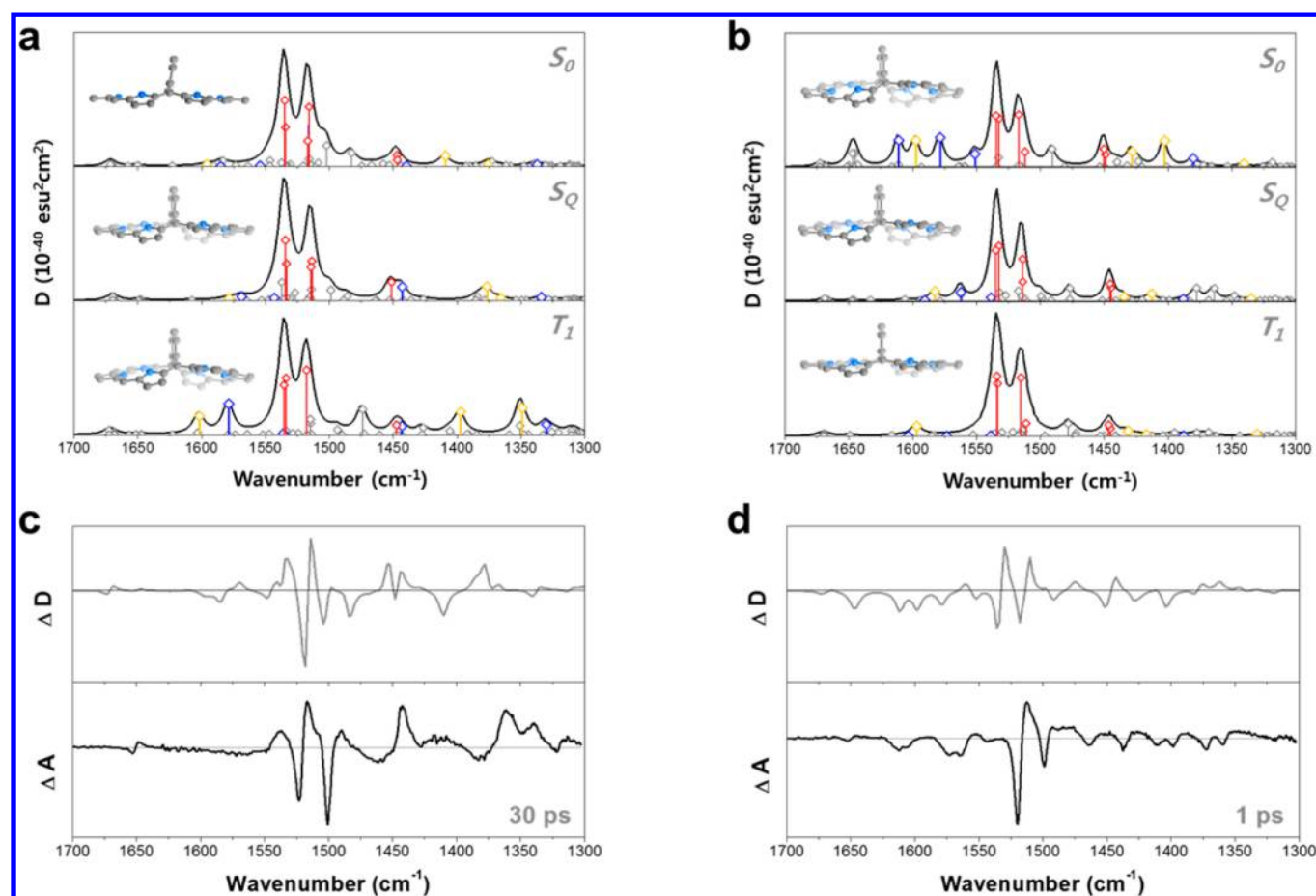


**Figure 9.** (a, b) Calculated IR spectra of the  $S_0$ ,  $S_Q$ , and  $T_1$  states and (insets) optimized structures of (a) 8 and (b) 9. The *meso*- $\text{C}_6\text{F}_5$  substituents and hydrogen atoms in the structures have been omitted for clarity. The IR bands marked in red indicate vibrational modes from the *meso*- $\text{C}_6\text{F}_5$  substituents. The IR bands marked in blue and yellow are the matched symmetric and asymmetric stretching modes. Both are intensified and attenuated according to structural distortion and planarization, respectively). (c, d) Simulated (top) and experimental (bottom) TRIR spectra of (c) 8 and (d) 9. Reprinted with permission from ref 5. Copyright 2017 Elsevier.

hexaphyrin framework. Thus, the interconvertible IR absorption features between the FTIR and TRIR spectra of 8 and 9 are interpreted in the same way as those of 1 and 2 on the basis of the IR activity of  $\text{C}=\text{C}$  stretching modes. The negligible IR absorption features of 8 in the ground state and 9 in the excited singlet state illustrate their planar and symmetric structures, while additional bands of 8 in the excited singlet state (at 1340, 1360, 1440, and  $1540 \text{ cm}^{-1}$ ) and 9 in the ground state (at 1375, 1400, 1570, and  $1615 \text{ cm}^{-1}$ ) indicate the asymmetric and out-of-plane  $\text{C}=\text{C}$  stretching modes arising from their distorted structures, which describe well the structural changes of 8 and 9 driven by the reversed aromaticity in the excited singlet states.<sup>14</sup>

The quantum-mechanical calculations give a comprehensive understanding of the correlation between the IR spectral features and the aromaticity. The calculated ground-state IR spectra of aromatic 1, antiaromatic 2, aromatic 8, and antiaromatic 9, which are well-matched with their FTIR spectra, signify that the common IR bands at 1430, 1485, 1520, and  $1650 \text{ cm}^{-1}$  originate from the local asymmetric  $\text{C}=\text{C}$  stretching modes of the *meso*- $\text{C}_6\text{F}_5$  substituents (Figure 9). Since the simulated TRIR spectra are in good accordance with the experimental ones, the qualitative analyses of the IR bands of 1, 2, 8, and 9 in the ground and excited states by approximating the hexaphyrin framework as having  $D_{2h}$  symmetry illustrate the IR activity of the  $\text{C}=\text{C}$  stretching

modes in association with molecular distortions.<sup>5,15</sup> The IR frequency calculation displays that the weak and negligible bands in the ground-state IR spectra of 1 and 8 arise from the symmetric in-plane  $\text{C}=\text{C}$  stretching motions along the main hexaphyrin  $\pi$ -conjugation pathway, which are also obtained in the calculations for 2 in the lowest triplet state and 9 in the excited singlet state.<sup>5</sup> In contrast, the asymmetric out-of-plane  $\text{C}=\text{C}$  stretching motions in the IR frequency calculations of 2 and 9 in the ground state show higher intensities. In addition, these IR-active asymmetric and out-of-plane stretching modes are observed in the frequency calculations of 1 and 8 in the lowest triplet and excited singlet states, respectively. These IR frequency analyses delineate that the IR activity of the  $\text{C}=\text{C}$  stretching modes is associated with the conformational distortion triggered by the reversal of aromaticity, which rationalizes the interconvertible IR spectra features between the FTIR and TRIR spectra. This suggests that the aromaticity reversal in the excited states can be observed by IR measurements, which will provide more accurate and reliable experimental information for the evaluation of aromaticity in excited states in combination with the electronic absorption spectral features in those excited states.

## CONCLUSIONS AND OUTLOOK

In this Account, a recent breakthrough for the evaluation of excited-state aromaticity in expanded porphyrins has been illustrated in terms of time-resolved optical spectroscopic measurements. Time-resolved electronic and vibrational absorption spectroscopies capture the changes in electronic structure and molecular conformation driven by the reversal of aromaticity, which experimentally demonstrate the aromaticity reversal and offer a new perspective to the field of excited-state aromaticity.

Furthermore, these new experimental approaches for studying excited-state aromaticity, namely, the correlation of optical spectral features with changes in  $\pi$ -electronic structure and molecular conformation induced by the reversal of aromaticity, will eventually set up a cornerstone providing direct insight into the role of (anti)aromaticity in the stability, dynamics, and reactivity in the excited states. Moreover, changes in molecular structure and aromaticity are a very important issue in the field of chemistry because they are one of the major and powerful driving forces to control and modulate molecular properties, where many distinct switchable molecular behaviors are involved in the altered conformation and aromaticity. Thus, understanding the role of excited-state aromaticity in structural changes and accompanying stabilization/destabilization of molecules upon irradiation enables mechanistic elucidation of photoinduced properties and its application to synthetic protocols and photoactive materials.<sup>4,7,9,37</sup> In this regard, the time-resolved optical spectroscopic approaches will act as a guideline for applications in designing photosynthetic protocols and photoactive materials as well as investigations of excited-state aromaticity.

## AUTHOR INFORMATION

### Corresponding Author

\*E-mail: dongho@yonsei.ac.kr

### ORCID

Dongho Kim: 0000-0001-8668-2644

### Present Address

<sup>†</sup>Y.M.S.: Samsung Advanced Institute of Technology, Samsung-ro 130, Yeongtong-gu, Suwon-si, Gyeonggi-do 18448, South Korea.

### Notes

The authors declare no competing financial interest.

### Biographies

**Juwon Oh** received a B.S. and is currently a Ph.D. candidate at Yonsei University.

**Young Mo Sung** received his Ph.D. (2015) and worked as a postdoctoral associate at Yonsei University. He received the S-oil Outstanding Dissertation Award (2015). He is currently a researcher at Samsung Advanced Institute of Technology.

**Yongseok Hong** received a B.S. and is currently a Ph.D. candidate at Yonsei University.

**Dongho Kim** received his B.S. in 1980 from Seoul National University and his Ph.D. in 1984 from Washington University. He joined the Korea Research Institute of Standards and Science in 1986. In 2000 he moved to Yonsei University as a Professor and is now Underwood Distinguished Professor. He has received the Scientist of the Month Award (1999), the Sigma-Aldrich Award (2005), the Korea Science Award in Chemistry (2006), the National Science Achieving

Excellence Award (2010), and the FILA Basic Science Award (2017). His research has focused on molecular excited-state properties and dynamics. He is a member of the editorial boards for the *Journal of Porphyrins and Phthalocyanines* and *The Journal of Physical Chemistry*.

## ACKNOWLEDGMENTS

First, we thank colleagues with whom we have been collaborating on this subject, in particular Prof. Atsuhiko Osuka (Kyoto University) and his research fellows. The work described in this Account was supported by the Samsung Science and Technology Foundation under Project SSTF-BA1402-10. The quantum calculations were performed using the supercomputing resources of the Korea Institute of Science and Technology Information (KISTI).

## REFERENCES

- (1) Hückel, E. Zur Quantentheorie der Doppelbindung. *Eur. Phys. J. A* **1931**, *70*, 204–286.
- (2) Baird, N. C. Quantum Organic Photochemistry. II. Resonance and Aromaticity in the Lowest  ${}^3\pi\pi^*$  State of Cyclic Hydrocarbons. *J. Am. Chem. Soc.* **1972**, *94*, 4941–4948.
- (3) Rosenberg, M.; Dahlstrand, C.; Kilså, K.; Ottosson, H. Excited State Aromaticity and Antiaromaticity: Opportunities for Photo-physical and Photochemical Rationalizations. *Chem. Rev.* **2014**, *114*, 5379–5425.
- (4) Sung, Y. M.; Oh, J.; Cha, W.-Y.; Kim, W.; Lim, J. M.; Yoon, M.-C.; Kim, D. Control and Switching of Aromaticity in Various All-Aza-Expanded Porphyrins: Spectroscopic and Theoretical Analyses. *Chem. Rev.* **2017**, *117*, 2257–2312.
- (5) Oh, J.; Sung, Y. M.; Mori, H.; Park, S.; Jorner, K.; Ottosson, H.; Lim, M.; Osuka, A.; Kim, D. Unraveling Excited-Singlet-State Aromaticity via Vibrational Analysis. *Chem* **2017**, *3*, 870–880.
- (6) Zeng, W.; Phan, H.; Heng, T. S.; Gopalakrishna, T. Y.; Aratani, N.; Zeng, Z.; Yamada, H.; Ding, J.; Wu, J. Rylene Ribbons with Unusual Diradical Character. *Chem* **2017**, *2*, 81–92.
- (7) Streifel, B. C.; Zafra, J. L.; Espejo, G. L.; Gómez-García, C. J.; Casado, J.; Tovar, J. D. An Unusually Small Singlet-Triplet Gap in a Quinoidal 1,6-Methano[10]annulene Resulting from Baird's  $4n$   $\pi$ -Electron Triplet Stabilization. *Angew. Chem., Int. Ed.* **2015**, *54*, 5888–5893.
- (8) Cha, W.-Y.; Kim, T.; Ghosh, A.; Zhang, Z.; Ke, X.-S.; Ali, R.; Lynch, V. M.; Jung, J.; Kim, W.; Lee, S.; Fukuzumi, S.; Park, J. S.; Sessler, J. L.; Chandrashekar, T. K.; Kim, D. Bicyclic Baird-Type Aromaticity. *Nat. Chem.* **2017**, *9*, 1243–1248.
- (9) Papadakis, R.; Ottosson, H. The excited state antiaromatic benzene ring: a molecular Mr Hyde? *Chem. Soc. Rev.* **2015**, *44*, 6472–6493.
- (10) Löfås, H.; Jahn, B. O.; Wärnå, J.; Emanuelsson, R.; Ahuja, R.; Grigoriev, A.; Ottosson, H. A computational study of potential molecular switches that exploit Baird's rule on excited-state aromaticity and antiaromaticity. *Faraday Discuss.* **2014**, *174*, 105–124.
- (11) Sung, Y. M.; Yoon, M.-C.; Lim, J. M.; Rath, H.; Naoda, K.; Osuka, A.; Kim, D. Reversal of Hückel (anti)aromaticity in the Lowest Triplet States of Hexaphyrins and Spectroscopic Evidence for Baird's Rule. *Nat. Chem.* **2015**, *7*, 418–422.
- (12) Oh, J.; Sung, Y. M.; Kim, W.; Mori, S.; Osuka, A.; Kim, D. Aromaticity Reversal in the Lowest Excited Triplet State of Archetypical Möbius Heteroannulenic Systems. *Angew. Chem., Int. Ed.* **2016**, *55*, 6487–6491.
- (13) Hong, Y.; Oh, J.; Sung, Y. M.; Tanaka, Y.; Osuka, A.; Kim, D. The Extension of Baird's Rule to Twisted Heteroannulenes: Aromaticity Reversal of Singly and Doubly Twisted Molecular Systems in the Lowest Triplet State. *Angew. Chem., Int. Ed.* **2017**, *56*, 2932–2936.
- (14) Sung, Y. M.; Oh, J.; Kim, W.; Mori, H.; Osuka, A.; Kim, D. Switching between Aromatic and Antiaromatic 1,3-Phenylene-

Strapped [26]- and [28]Hexaphyrins upon Passage to the Singlet Excited State. *J. Am. Chem. Soc.* **2015**, *137*, 11856–11859.

(15) Sung, Y. M.; Oh, J.; Naoda, K.; Lee, T.; Kim, W.; Lim, M.; Osuka, A.; Kim, D. A Description of Vibrational Modes in Hexaphyrins: Understanding the Aromaticity Reversal in the Lowest Triplet State. *Angew. Chem., Int. Ed.* **2016**, *55*, 11930–11934.

(16) Ueda, M.; Jorner, K.; Sung, Y. M.; Mori, T.; Xiao, Q.; Kim, D.; Ottosson, H.; Aida, T.; Itoh, Y. Energetics of Baird Aromaticity Supported by Inversion of Photoexcited Chiral [4*n*]annulene Derivatives. *Nat. Commun.* **2017**, *8*, 346.

(17) Kim, S.; Park, J.; Lee, T.; Lim, M. Direct Observation of Ligand Rebinding Pathways in Hemoglobin Using Femtosecond Mid-IR Spectroscopy. *J. Phys. Chem. B* **2012**, *116*, 6346–6355.

(18) Dean, J. C.; Mirkovic, T.; Toa, Z. S. D.; Oblinsky, D. G.; Scholes, G. D. Vibronic Enhancement of Algae Light Harvesting. *Chem.* **2016**, *1*, 858–872.

(19) Yoon, Z. S.; Osuka, A.; Kim, D. Möbius Aromaticity and Antiaromaticity in Expanded Porphyrins. *Nat. Chem.* **2009**, *1*, 113–122.

(20) Shin, J.-Y.; Kim, K. S.; Yoon, M.-C.; Lim, J. M.; Yoon, Z. S.; Osuka, A.; Kim, D. Aromaticity and Photophysical Properties of Various Topology-Controlled Expanded Porphyrins. *Chem. Soc. Rev.* **2010**, *39*, 2751–2767.

(21) Cho, S.; Yoon, Z. S.; Kim, K. S.; Yoon, M. C.; Cho, D. G.; Sessler, J. L.; Kim, D. Defining Spectroscopic Features of Heteroannulenic Antiaromatic Porphyrinoids. *J. Phys. Chem. Lett.* **2010**, *1*, 895–900.

(22) Hada, M.; Saito, S.; Tanaka, S.; Sato, R.; Yoshimura, M.; Mouri, K.; Matsuo, K.; Yamaguchi, S.; Hara, M.; Hayashi, Y.; Röhricht, F.; Herges, R.; Shigeta, Y.; Onda, K.; Miller, R. J. D. Structural Monitoring of the Onset of Excited-State Aromaticity in a Liquid Crystal Phase. *J. Am. Chem. Soc.* **2017**, *139*, 15792–15800.

(23) Sessler, J. L.; Seidel, D. Synthetic Expanded Porphyrin Chemistry. *Angew. Chem., Int. Ed.* **2003**, *42*, 5134–5175.

(24) Oh, J.; Mori, H.; Sung, Y. M.; Kim, W.; Osuka, A.; Kim, D. Switchable  $\pi$ -Electronic Network of Bis( $\alpha$ -Oligothieryl)-Substituted Hexaphyrins between Helical versus Rectangular Circuit. *Chem. Sci.* **2016**, *7*, 2239–2245.

(25) Jana, A.; Ishida, M.; Park, J. S.; Bähring, S.; Jeppesen, J. O.; Sessler, J. L. Tetrathiafulvalene- (TTF-) Derived Oligopyrrolic Macrocycles. *Chem. Rev.* **2017**, *117*, 2641–2710.

(26) Mulugeta, E.; He, Q.; Sareen, D.; Hong, S.-J.; Oh, J. H.; Lynch, V. M.; Sessler, J. L.; Kim, S. K.; Lee, C.-H. Recognition, Sensing, and Trapping of Bicarbonate anions with a Dicationic *meso*-Bis-(benzimidazolium) Calix[4]pyrrole. *Chem.* **2017**, *3*, 1008–1020.

(27) Gouterman, M. Spectra of Porphyrins. *J. Mol. Spectrosc.* **1961**, *6*, 138–163.

(28) Yoon, M. C.; Cho, S.; Suzuki, M.; Osuka, A.; Kim, D. Aromatic versus Antiaromatic Effect on Photophysical Properties of Conformationally Locked *trans*-Vinylene-Bridged Hexaphyrins. *J. Am. Chem. Soc.* **2009**, *131*, 7360–7367.

(29) Muranaka, A.; Matsushita, O.; Yoshida, K.; Mori, S.; Suzuki, M.; Furuyama, T.; Uchiyama, M.; Osuka, A.; Kobayashi, N. Application of the Perimeter Model to the Assignment of the Electronic Absorption Spectra of Gold(III) Hexaphyrins with [4*n*+2] and [4*n*]  $\pi$ -Electron Systems. *Chem. - Eur. J.* **2009**, *15*, 3744–3751.

(30) Heilbronner, E. Hückel Molecular Orbitals of Möbius-Type Conformations of Annulenes. *Tetrahedron Lett.* **1964**, *5*, 1923–1928.

(31) Karadakov, P. B. Ground- and Excited-State Aromaticity and Antiaromaticity in Benzene and Cyclobutadiene. *J. Phys. Chem. A* **2008**, *112*, 7303–7309.

(32) Karadakov, P. B.; Hearnshaw, P.; Horner, K. E. Magnetic Shielding, Aromaticity, Antiaromaticity, and Bonding in the Low-Lying Electronic States of Benzene and Cyclobutadiene. *J. Org. Chem.* **2016**, *81*, 11346–11352.

(33) Setiawan, D.; Kraka, E.; Cremer, D. Quantitative Assessment of Aromaticity and Antiaromaticity Utilizing Vibrational Spectroscopy. *J. Org. Chem.* **2016**, *81*, 9669–9686.

(34) Garavelli, M.; Bernardi, F.; Cembran, A.; Castaño, O.; Frutos, L. M.; Merchán, M.; Olivucci, M. Cyclooctatetraene Computational Photo- and Thermal Chemistry: A Reactivity Model for Conjugated Hydrocarbons. *J. Am. Chem. Soc.* **2002**, *124*, 13770–13789.

(35) Krygowski, T. M.; Cyrański, M. K. Structural Aspects of Aromaticity. *Chem. Rev.* **2001**, *101*, 1385–1419.

(36) Kalescky, R.; Kraka, E.; Cremer, D. Description of Aromaticity with the Help of Vibrational Spectroscopy: Anthracene and Phenanthrene. *J. Phys. Chem. A* **2014**, *118*, 223–237.

(37) Jorner, K.; Dreos, A.; Emanuelsson, R.; El Bakouri, O.; Galván, I. F.; Börjesson, K.; Feixas, F.; Lindh, R.; Zietz, B.; Moth-Poulsen, K.; Ottosson, H. Unraveling factors leading to efficient norbornadiene-quadracycline molecular solar-thermal energy storage systems. *J. Mater. Chem. A* **2017**, *5*, 12369–12378.